Specificity of the Local Structure of Nanocrystalline Doped Ceria Solid Electrolytes

Vladislav A. Sadykov, Yulia V. Frolova, Vladimir V. Kriventsov, Dmitrii I. Kochubei, Ella M. Moroz, Dmitrii A. Zyuzin, Yulia V. Potapova, Vitalii S. Muzykantov, Vladimir I. Zaikovskii, Elena B. Burgina, Holger Borchert, Sergei Trukhan, Vyacheslav P. Ivanov, Stylianos Neophytides[1], Erhard Kemnitz[2], Kerstin Scheurell[2]

Boreskov Institute of Catalysis SB RAS, Lavrentieva, 5, 630090, Novosibirsk, Russia
[1] Institute of High Temperature Processes & Chemical Engineering, GR-26500, Patras, Greece
[2] Institute of Chemistry, Humboldt University, Brook-Taylor-Str. 2, D-12489 Berlin, Germany

ABSTRACT

This work presents results of studies of the structural features of nanocrystalline doped $Ce_{1-x}Me_xO_{2-y}$ samples (Me = Sm, Bi, Gd; x = 0-0.5) prepared via the polymerised precursor (Pechini) route by using a combination of diffraction (XRD, TEM, WAXS on SR) and spectroscopic (EXAFS, Raman, FTIRS of lattice modes, XPS, SIMS) methods.

INTRODUCTION

Nanocrystalline ceria doped with low-valence cations is known to possess a high oxygen–ion conductivity due to the presence of anion vacancies [1]. This makes ceria-based systems attractive for various applications like intermediate-temperature solid oxide fuel cells [2], electrochemical oxygen pumps and components of oxygen-conducting membranes [3], catalytic systems for partial oxidation of methane or other hydrocarbons to syngas [4], etc. These applications are due to the possibility of easy sintering into mechanically strong dense ceramics as well as specific defect/transport properties associated with high surface/grain boundary areas. However, only little is known about the specificity of the real/defect structure of nanocrystalline doped ceria due to difficulties of its characterization by traditional diffraction methods.

The aim of this paper is the study of the real/defect structure of ceria doped with Bi, Sm and Gd cations by using more sophisticated diffraction and spectroscopic methods.

EXPERIMENTAL DETAILS

Dispersed samples of ceria-based solid solutions with Sm, Bi or Gd content in the range of 10–50 at.% were prepared by a polymerized complex precursor route as in [5, 6] and calcined at 500 ^oC. Samples were characterized by X-ray Diffraction (XRD), Transmission Electron Microscopy (TEM), Wide-Angle X-ray Scattering (WAXS) on synchrotron radiation (SR) as well as by spectroscopic methods such as Extended X-ray Absorption Fine Structure Spectroscopy (EXAFS), Raman, Fourier –transform Spectroscopy of Lattice Modes (FTIRS), X-ray Photoelectron Spectroscopy (XPS), and Secondary Ions Mass-Spectrometry (SIMS).

XRD experiments were performed using an URD-6 diffractometer with monochromatized Cu K_α radiation, and a JEOL JEM-2010 transmission electron microscope operating at 200kV was used for TEM studies [6]. The EXAFS spectra of the Ce-L_3, Sm-L_3, Gd-L_3 and Bi-L_3 edges were obtained at the EXAFS Station of the Siberian Synchrotron Radiation Center. The storage

ring VEPP-3 with an electron beam energy of 2 GeV and an average stored current of 90 mA has been used as the source of radiation. The X-ray energy was monitored with a channel cut Si(111) monochromator. All the spectra were recorded under transmission mode using two ionization chambers as detectors. The harmonic rejection was performed by using a gold mirror. The EXAFS spectra were analysed using standard procedures [7]. FTIRS of lattice modes experiments were carried out on a BOMEM MB-12 IR-Fourier spectrometer in the 4000-250 cm^{-1} wavenumber range. Raman spectra were recorded with a Raman Fourier spectrometer 100/S Bruker. XPS measurements of Gd-doped ceria samples were performed with a VG ESCALAB HP spectrometer using Al K_α radiation. Powder samples were pressed into spoon-like copper sample holders and treated with oxygen (exposure for 1 h to 5000 Pa O_2 at 400° C) in the preparation chamber of the spectrometer before spectra were measured at room temperature. SIMS experiments were carried out as described in Ref. [8] where the signals at m/e values of 140 and 160 were assigned to secondary ion currents of cerium and gadolinium ions, respectively. Oxygen mobility up to 700 ^oC was estimated by using isotope exchange both in dynamic and isothermal conditions [9].

RESULTS AND DISCUSSION

As revealed by powder X-ray diffraction, all of the doped ceria samples are single-phase fluorite-like solid solutions. The lattice constant increases approximately linearly with the dopant content where the slope depends on the doping element (see Figure 1a). The effect is quantitatively in good agreement with results reported by McBride et al. [10] for Gd- and Sm-doped ceria and can be understood in terms of ionic radii of the host and guest cations. According to Shannon, Ce^{4+} cation has the ionic radius of 0.97 Å, while the ionic radii of the Me^{3+} guest cations are larger: 1.17 Å for Bi^{3+}, 1.079 Å for Sm^{3+} and 1.053 Å for Gd^{3+} [11].

TEM analysis has shown that the doped ceria samples consist of nanocrystalline domains sintered together thus forming a developed network of disordered domain boundaries. The average size of the nanocrystalline domains has been determined by XRD and turned out to decline with increasing the dopant content (see Figure 1b). This is probably due to segregation of dopant cations at the domain surface which hinders its further growth.

The local structure around Ce and dopant cations was studied by EXAFS and WAXS using synchrotron radiation. It was found to be strongly distorted even in pure nanocrystalline ceria [12] and to depend on the type and amount of dopant cations as well. Progressive disordering of the lattice with increasing dopant content is reflected in decline of the intensities of EXAFS peaks. At a high dopant content, a local rearrangement of the structure into that of a lower symmetry is reflected in appearance of new EXAFS peaks [12]. Figure 2 shows the relative intensities of Ce-O (a) and Ce-Me (b) peaks of EXAFS spectra of the Ce-L_3 edge. The analysis of the amplitudes of peaks assigned to different coordination spheres and investigations of the corresponding distances revealed the most uniform distribution in the ceria lattice for the smallest Gd cations. In addition, for Gd-doped ceria, anion vacancies appear to be preferentially located in the coordination sphere of Ce cations, whereas they are mainly associated with the guest cations in the case of a larger dopant (Sm, Bi).

Figure 3 shows Raman spectra of $Ce_{1-x}Gd_xO_{2-y}$ and $Ce_{1-x}Bi_xO_{2-y}$ systems. For all samples, increasing dopant content results in a decline of the peak intensity. The absolute peak intensity is higher for the $Ce_{1-x}Bi_xO_{2-y}$ system than for the $Ce_{1-x}Gd_xO_{2-y}$ system. With increasing dopant content the band position shifts to higher frequencies for the $Ce_{1-x}Gd_xO_{2-y}$ system while a shift to

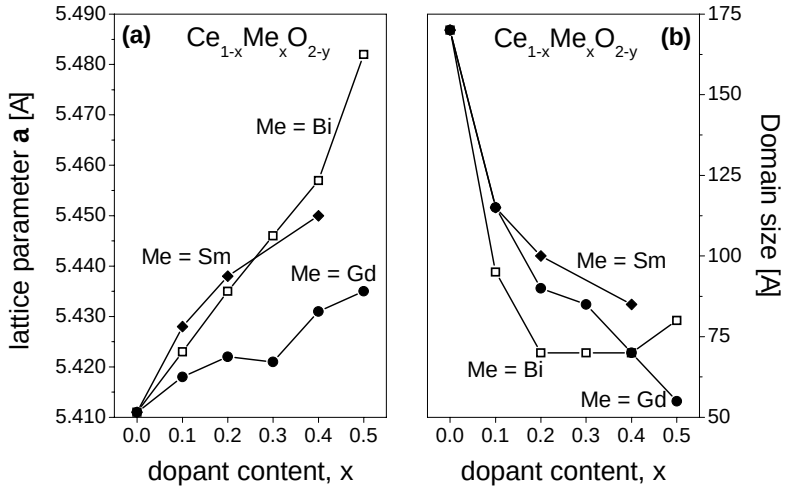

Figure 1. Dependence of the lattice parameter (a) and the domain size (b) of nanocrystalline doped ceria samples on the type and content of a dopant.

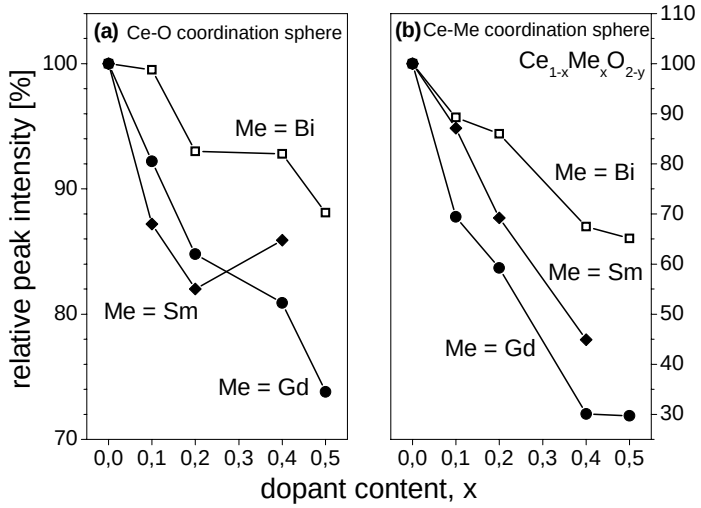

Figure 2. Relative intensities of Ce-O (a) and Ce-Me (b) peaks of EXAFS spectra of the Ce-L_3 edge. CeO_2 has been used as reference.

lower frequencies is observed for Bi-doped ceria. This provides evidence for a local rearrangement of the structure at a high dopant content.

For $Ce_{1-x}Sm_xO_{2-y}$ system, at a low dopant content, the peak intensity also declines. However, at the highest doping level, for this system the intensity increases again due to a local rearrangement of the structure into that of a lower symmetry as revealed by WAXS [12].

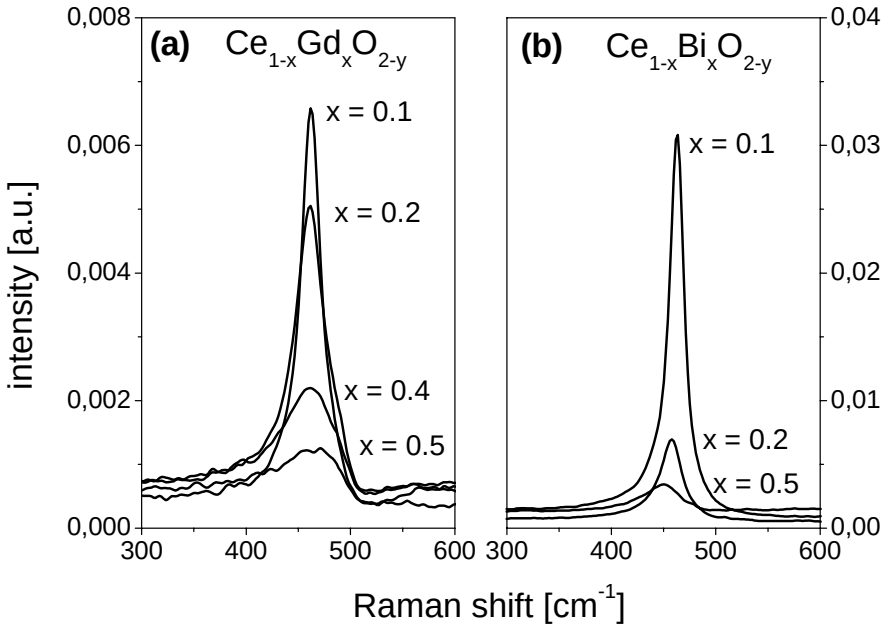

Figure 3. Raman spectra of the nanostructured ceria samples doped with (a) Gd and (b) Bi as dependent on the dopant content.

Segregation of dopant ions at the surface has been studied by SIMS and XPS [13]. Figure 4 shows the ratio of the secondary ion currents corresponding to Gd and Ce ions for samples with 10% to 50% gadolinium content as a function of sputtering depth. For all samples an enhanced ion current ratio is observed at the beginning of the sputtering which provides a clear indication for segregation of gadolinium ions at the surface. In all cases, after removal of about ~1 nm of substance, the ion current ratio reaches a more or less constant level which indicates a rather homogeneous distribution of the dopant ions in the volume of the nanocrystalline domains.

Segregation of gadolinium ions at the surface was confirmed by XPS. For all samples, the atomic ratio of Gd to Ce as determined from the Gd 3d and Ce 3d peak areas (corrected for the corresponding sensitive factors) significantly exceeded the theoretical value for the case of homogeneous distribution of the dopant ions in the host lattice [13]. A similar situation was observed for Bi-doped ceria samples where Bi 4f and Ce 3d peak areas have been evaluated.

The lattice oxygen mobility was estimated by oxygen dynamic isotope exchange in the temperature-programmed regime. For all samples, 3rd type of exchange (two surface oxygen atoms take part in the exchange) was shown to dominate [12]. For $Ce_{1-x}Gd_xO_{2-y}$ and $Ce_{1-x}Sm_xO_{2-y}$ systems the amount of exchangeable oxygen goes through the maximum at a low dopant content (x=0.2). It correlates with the density of free anion vacancies located in the coordination sphere of Ce cations. The amount of exchangeable oxygen is higher for the $Ce_{0.8}Gd_{0.2}O_{2-y}$ system (X_s ~9 monolayers) and oxygen isotope exchange starts at lower temperature (450° C) than in case of Sm-doped ceria (X_s~2 monolayers and 500° C) (see Figure 5).

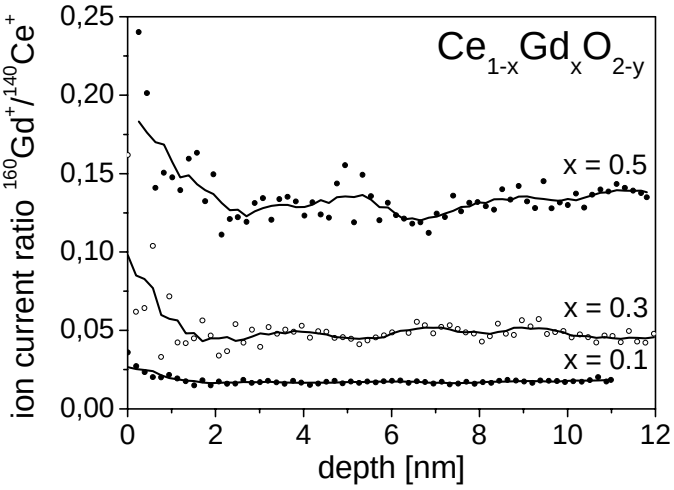

Figure 4. Ratio of the secondary ion currents corresponding to Gd and Ce for doped ceria samples with different Gd content. The raw data (points) are plotted together with smoothed curves (lines) to guide the eye.

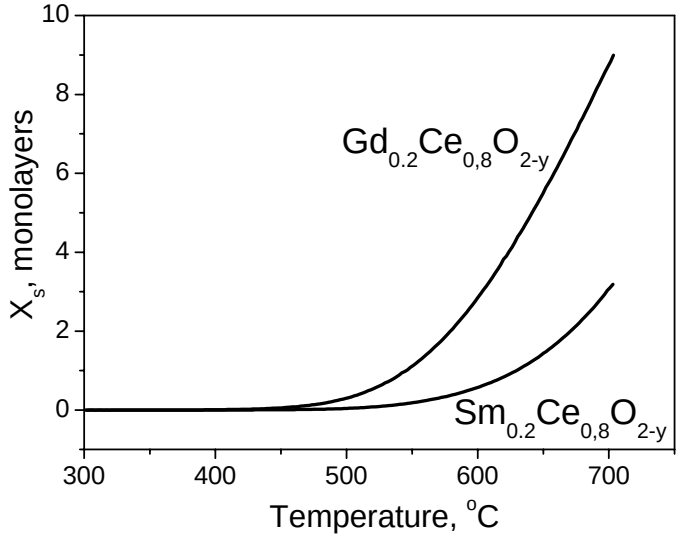

Figure 5. Dynamic extent of the isotopic exchange X_s versus temperature for $Ce_{0,8}Gd_{0.2}O_{2-y}$ and $Ce_{0,8}Sm_{0.2}O_{2-y}$ samples. $X_s = \lambda_s \{(\alpha^o/\alpha)-1\}$, where $\lambda_s=N/N_s$ (monolayers), N - number of O atoms in the gas phase; N_s- number of exchangeable oxygen atoms in the oxide monolayer, α^o, α- initial and current fraction of ^{18}O in the gas phase.

CONCLUSIONS

For nanocrystalline ceria samples doped with Gd, Sm and Bi cations prepared via Pechini route, a single-phase fluorite-like solid solution is formed up to the dopant content 50 at.%. Hence, Pechini route ensures rather homogeneous distribution of a dopant in the ceria lattice, though some dopant segregation in the surface layer was revealed. At a high doping level, a strong rearrangement of the local structure around both Ce and dopant cations occurs being more extensive for dopants with bigger sizes. This results in decreasing the concentration of free anion vacancies in the lattice determining the lattice oxygen mobility.

ACKNOWLEDGMENTS

This work is in part supported by the INTAS 01-2162, ISTC 2529 Projects and Integration Projects 39 and 110 of SB RAS. Furthermore, a DAAD postdoctoral research fellowship to H.B. is acknowledged.

REFERENCES

1. H. Inaba, H. Tagawa, Solid State Ionics **83,** 1 (1996).
2. M. Mogensen, N. M. Sammes, G. A. Tompsett, Solid State Ionics **129**, 63 (2000).
3. U. Nigge, H.-D. Wiemhöfer, E. W. J. Römer, H. J. M. Bouwmeester, T. R. Schulte, Solid State Ionics **146**, 163 (2002).
4. M. Krumpelt, Sh. Ahmed, R. Kumar, R. Doshi, U.S. Patent 6,110,861 (2000).
5. M. P. Pechini: U.S. Patent 3,330,697 (1967).
6. T. G. Kuznetsova, V. A. Sadykov, E. M. Moroz, S. N. Trukhan, E. A. Paukshtis, V. N. Kolomiichuk, E. B. Burgina, V. I. Zaikovskii, M. A. Fedotov, V. V. Lunin, E. Kemnitz. Stud. Surf. Sci. Catal. **143**, 659 (2002).
7. D. I. Kochubey, EXAFS spectroscopy of catalysts, Nauka, Novosibirsk, 1992.
8. H. Borchert, Y. V. Frolova, V. V. Kaichev, I. P. Prosvirin, G. M. Alikina, A. I. Lukashevich, V. I. Zaikovskii, E. M. Moroz, S. N. Trukhan, V. P. Ivanov, E. A. Paukshtis, V. I. Bukhtiyarov, V. A. Sadykov, J. Phys. Chem. B, submitted.
9. V. S. Muzykantov, V. A. Sadykov, E. Kemnitz, V. V. Lunin, Kinetika I Kataliz **44**, 349 (2003)
10. J. R. McBride, K. C. Hass, B. D. Poindexter, W. H. Weber, J. Appl. Phys. **76**, 2435 (1994).
11. R. D. Shannon, Acta Cryst. A **32**, 751 (1976).
12. V. A. Sadykov, T. G. Kuznetsova, G. M. Alikina, Yu. V. Frolova, A. I. Lukashevich, Yu. V. Potapova, V. S. Muzykantov, V. A. Rogov, V. V. Kriventsov, D. I. Kochubei, E. M. Moroz, D. I. Zuzin, V. I. Zaikovskii, V. N. Kolomiichuk, E. A. Paukshtis, E. B. Burgina, V. V. Zyryanov, N. F. Uvarov, S. Neophytides, E. Kemnitz, Catalysis Today **93-95**, 45 (2004).
13. V. A.Sadykov, Yu. V. Frolova, G. M. Alikina, A. I. Lukashevich, V. S. Muzykantov, V. A. Rogov, E. M. Moroz, D. A. Zyuzin, V. P. Ivanov, S. N. Trukhan, V. I. Zaikovskii, H. Borchert, E. A. Paukshtis, V. I. Bukhtiyarov, V. V. Kaichev, I. P. Prosvirin, S. Neophytides, E. Kemnitz, K. Scheurell, React. Kinet. Catal. Lett., accepted.